STATIC AND DYNAMIC ANALYSIS OF 2-D FUNCTIONALLY GRADED ELASTICITY BY USING MESHLESS LOCAL PETROV-GALERKIN METHOD

Ling-Fang Qian and Hsu-Kuang Ching*

ABSTRACT

Numerical solutions obtained by the Meshless Local Petrov-Galerkin (MLPG) method are presented for static deformations, free and forced vibrations of a functionally graded (FG) cantilever beam. The MLPG method is a truly meshless approach, as it does not need any background mesh for integration in the weak form. In this MLPG method, an orthogonal transformation technique is used to enforce nodal variables directly in the essential boundary areas, and the test function is chosen to equal the weight function of the moving least squares approximation. The cantilever beam, made of two isotropic constituents, is assumed to be macroscopically isotropic and to have a power-law variation proportional to the volume fractions of the constituents in the thickness and the longitudinal directions. Effective material moduli at a material point are computed with the Mori-Tanaka homogenization technique. Computed results for static, free and forced vibration analyses are found to agree well with their corresponding finite element solutions. Different volume fractions of material constituents on the performance and response of FG beams are also investigated.

Key Words: meshless method, MLPG, functionally graded materials, natural frequencies, cantilever beam.

I. INTRODUCTION

Functionally graded materials (FGMs) are a new class of advanced composite materials wherein the composition of each material constituent varies gradually with respect to spatial coordinates. FGMs possess continuously and smoothly varying material properties, and this distinguishes FGMs from laminated composite materials in which the abrupt change in material properties across the interfaces between layers can result in large interlaminar stresses leading to delamination. The materials are made to utilize desirable properties of their individual constituents. For example, thermal protection plate structures made of a two-phase ceramic/metal functionally graded composite provide heat and corrosion resistance on the ceramic-rich surface while maintaining structural strength and stiffness provided by the metal-rich surface. Moreover, FGMs allow for tailoring the volume fractions of two or more constituents to optimize the performance of structures. If properly designed, FGMs can offer various advantages such as reduction of thermal stresses, minimization of stress concentration or intensity factors and attenuation of stress waves. As such, FGMs have gained widespread uses in a different range of engineering components or systems where typical applications are aircraft fuselages in the aerospace industry, rocking-motor casings in the military industry, packaging materials in the microelectronic industry, engine components in the automotive industry, human implants in the biomedical industry and so on. A comprehensive review of design, processing, and modeling as well as applications of FGMs can be found in books by Suresh and Mortensen (1998), and by Miyamoto *et al*. (1999).

Several analytical solutions have been presented for the analysis of functionally graded (FG) structures. Delale and Erdogan (1983) derived the crack-tip stress

*Corresponding author. (Email: hching@siu.edu)

L. F. Qian is with the Nanjing University of Science and Technology, Nanjing 210094, P. R. China.

H. K. Ching is with the Materials Technology Center, Southern Illinois University, Carbondale, IL 62901, USA.

fields for an inhomogeneous solid under mechanical load by assuming the shear modulus varying with an exponential function. Noda and Jin (1993) computed the steady thermal stress intensity factor (TSIF) for inhomogeneous materials with exponential variations of thermal properties. Jin and Noda (1994) also calculated the TSIF under transient thermal loading. Jin and Batra (1996) used the two-dimensional (2-D) thermoelasticity theory to study fracture characteristics at a crack tip in an FG plate. Sankar (2001) proposed an elasticity solution for an FG beam in which the Young's modulus is assumed by the exponent function along the thickness. Tarn (2001) developed an exact solution for an FG anisotropic cylinder where the temperature distribution, deformations and stress fields are determined with power-law variations of thermoelastic constants. Deformations of FG plates have also been conducted by higher-order plate theories. Reddy (2000) presented solutions for rectangular FG plates based on the third-order shear deformation theory (TSDT). Cheng and Batra (2000) have related deflections of a simply supported functionally graded polygonal plate given by a TSDT and the first-order shear deformation theory (FSDT) to that of an equivalent homogeneous Kirchhoff plate. Vel and Batra (2002) provided an exact solution for the three-dimensional thermoelastic deformations of a simply supported FG plate with a power-law variation of the volume fractions of the constituents through the thickness.

Although analytical approaches provide closed-form solutions, they are limited to simple geometries, certain types of gradation of material properties (e.g. exponential or power-law distribution), specific types of boundary conditions (e.g. simple support) and special loading cases (e.g. sinusoidal loading).

In recent years, the meshless method has emerged as an effective numerical approach to find solutions of initial-boundary-value problems. The feature of this method is that only a set of scattered nodes is required in the physical domain to approximate solutions and nodes need not be connected to form closed polygons. In contrast to the finite element method (FEM), the meshless method can save the pre-processing work of mesh generation, as no element is required in the entire model. Besides, the computed stresses and strains are smooth without using any post-processing technique. More importantly, the material variation in FGMs can be captured at the level of the integration points whereas the conventional FEM treats inhomogeneous materials as numerous homogeneous elements and thereby a very fine mesh is required in the analysis of FGMs. A variety of different meshless methods have been proposed in the past few years such as the Diffuse Element Method (DEM) (Nayroles *et al*., 1992), the Element-Free Galerkin (EFG) method (Belytschko *et al*., 1994), the Hp-Clouds (Duarte and Oden, 1996), the Reproducing Kernel Particle Method (RKPM) (Liu *et al*., 1995), the Partition of Unity Finite Element Method (PUFEM) (Melenk and Babuska, 1996), and the Meshless Local Petrov-Galerkin (MLPG) method (Atluri and Zhu, 1998). The major difference among these methods lies in the interpolation techniques. We refer the reader to the work by Belytschko *et al*. (1996), and Atluri *et al*. (1999) for a review about the similarities and differences in various meshless methods.

The MLPG method is one of the meshless schemes. The main advantage of this method compared with other meshless methods is that no background mesh is used to evaluate various integrals appearing in the local weak formulation of a problem. Therefore, this method is a "truly meshless" approach in terms of both interpolation of variables and integration of energy. The MLPG method has been demonstrated to be quite successful in solving different branches of initial-boundary-value problems. The recent developments in the MLPG method include the following: Atluri and Zhu (2000) solved elastostatic problems, Lin and Atluri (2000) introduced the upwinding scheme to analyze steady state convection-diffusion problems, and Liu and Gu (2000) coupled the MLPG method with either the finite element or the boundary element method to enhance the efficiency of the MLPG method. Ching and Batra (2001) augmented the polynomial basis functions with singular fields to determine deformations and stress fields near the crack tip for general 2-D mixed-mode problems. Gu and Liu (2001a) and Batra and Ching (2002) used the Newmark family of methods to analyze 2-D transient elastodynamic problems. The bending of a thin plate has been studied by Gu and Liu (2001b) and Long and Atluri (2002). By utilizing the radial basis functions in the MLPG method, Liu and Gu (2001) developed a local radial point interpolation method (LRPIM) for free vibration analyses of 2-D solids; the shape functions derived by the LRPIM possess delta function property. Warlock *et al*. (2002) scrutinized deformations of a material compressed in a rough rectangular cavity. More recently, Qian *et al*. (2003a,b) combined the MLPG method with a higher-order shear and normal deformable theory to analyze static deformations, free and forced vibrations of a thick rectangular plate. They also delineated the effect of different parameters on the quality of the MLPG solutions.

The objective of this paper is to present a numerical solution for static and dynamic deformations of FG elastic beams using the MLPG method. In Section II, basic governing equations are proposed and their weak formulations are derived. Section III

gives the numerical implementation of the MLPG method including the moving least squares (MLS) approximation, the semidiscrete governing equations, the imposition of essential boundary conditions and the time integration scheme. Estimation of effective material moduli by the Mori-Tanaka method is described. Results for static analysis, free and forced vibration analyses of a FG cantilever beam are reported in Section IV. Finally, conclusions are summarized in Section V.

II. FORMULATION OF THE PROBLEM

For a 2-D solid occupying the domain Ω bounded by Γ in the rectangular Cartesian coordinate $\boldsymbol{x}=\{x, y\}^T$, the governing equations, neglecting body forces, for the small displacement elastodynamics are given as

$$\nabla \cdot \boldsymbol{\sigma} = \rho \ddot{\boldsymbol{u}} \quad \text{in} \quad \Omega \times [0, t] \tag{1}$$

where $\boldsymbol{\sigma}$ is the stress tensor which corresponds to the displacement field $\boldsymbol{u}=\{u, v\}^T$; ∇ is the gradient operator defined by $\nabla=\{\partial/\partial x, \partial/\partial y\}^T$; ρ is the mass density, $\ddot{\boldsymbol{u}}$ the acceleration and t the time. Eq. (1) is supplemented with the following initial conditions:

$$\boldsymbol{u}(\boldsymbol{x}, 0)=\boldsymbol{u}^0(\boldsymbol{x}) \quad \text{in } \Omega \tag{2a}$$

$$\dot{\boldsymbol{u}}(\boldsymbol{x}, 0)=\dot{\boldsymbol{u}}^0(\boldsymbol{x}) \quad \text{in } \Omega \tag{2b}$$

and boundary conditions:

$$\boldsymbol{u}=\overline{\boldsymbol{u}} \quad \text{on } \Gamma_u \times [0, t] \tag{3a}$$

$$\boldsymbol{\sigma n}=\overline{\boldsymbol{t}} \quad \text{on } \Gamma_t \times [0, t] \tag{3b}$$

where $\boldsymbol{u}^0(\boldsymbol{x})$, $\dot{\boldsymbol{u}}^0(\boldsymbol{x})$, $\overline{\boldsymbol{u}}$, and $\overline{\boldsymbol{t}}$ denote initial displacements, initial velocities, prescribed displacements and tractions, respectively, and $\boldsymbol{n}$ is the unit outward normal to Ω.

Let $\tilde{\boldsymbol{u}}=\{\tilde{u}, \tilde{v}\}^T$ be two linearly independent functions defined on Ω. Multiplication of Eq. (1) expressing the balance of linear momentum in the x and y directions by $\tilde{u}$ and $\tilde{v}$ respectively, addition of the resulting two equations and use of the divergence theorem and boundary conditions (3b) give

$$\int_\Omega \tilde{\boldsymbol{\varepsilon}}^T \boldsymbol{\sigma} d\Omega - \int_{\Gamma_u} \tilde{\boldsymbol{u}}^T \boldsymbol{\sigma n} d\Gamma - \int_{\Gamma_t} \tilde{\boldsymbol{u}}^T \overline{\boldsymbol{t}}\, d\Gamma + \int_\Omega \rho \tilde{\boldsymbol{u}}^T \ddot{\boldsymbol{u}} d\Omega = 0 \tag{4}$$

Equation (4) is the weak form associated with Eq. (1) and (3a). The constitutive equation at a material point is

$$\boldsymbol{\sigma}=\{\sigma_{xx} \;\; \sigma_{yy} \;\; \sigma_{xy}\}^T=\boldsymbol{D\varepsilon} \tag{5}$$

where $\boldsymbol{D}$, the matrix of elastic constants, is a function of space coordinates $\boldsymbol{x}$. For a 2-D isotropic solid in the plane stress state, $\boldsymbol{D}$ is given by

$$\boldsymbol{D} = \frac{\overline{E}(\boldsymbol{x})}{1-\overline{\nu}(\boldsymbol{x})^2} \begin{bmatrix} 1 & \overline{\nu}(\boldsymbol{x}) & 0 \\ \overline{\nu}(\boldsymbol{x}) & 1 & 0 \\ 0 & 0 & (1-\overline{\nu}(\boldsymbol{x}))/2 \end{bmatrix} \tag{6}$$

and the strain-displacement relationship is

$$\boldsymbol{\varepsilon} = \begin{Bmatrix} \varepsilon_{xx} \\ \varepsilon_{yy} \\ \varepsilon_{xy} \end{Bmatrix} = \begin{Bmatrix} \dfrac{\partial u(\boldsymbol{x})}{\partial x} \\ \dfrac{\partial v(\boldsymbol{x})}{\partial y} \\ \dfrac{\partial v(\boldsymbol{x})}{\partial x} + \dfrac{\partial u(\boldsymbol{x})}{\partial y} \end{Bmatrix} \tag{7}$$

$\tilde{\boldsymbol{\varepsilon}}$ in Eq. (4) takes the same form as in Eq. (7) with the displacement components $\boldsymbol{u}=\{u, v\}^T$ replaced by $\tilde{\boldsymbol{u}}=\{\tilde{u}, \tilde{v}\}^T$.

III. IMPLEMENTATION OF THE MLPG METHOD

1. Brief Description of the MLS Approximation

In the MLPG method, the basis functions $\phi_I(\boldsymbol{x})$ of the unknown trial function are found by the moving least squares (MLS) approximation; see Lancaster and Sallauska (1981) for details. For the sake of completeness, we briefly describe below the MLS approximation. Let $f(\boldsymbol{x}, t)$ be a scalar valued function defined on S_α; f can be identified with one of the displacements u or v. The approximation $f^h(\boldsymbol{x}, h)$ of f is assumed by

$$f^h(\boldsymbol{x}, t) = \boldsymbol{p}^T(\boldsymbol{x})\boldsymbol{a}(\boldsymbol{x}, t) = \sum_{J=1}^{m} p_J(\boldsymbol{x}) a_J(\boldsymbol{x}, t) \tag{8}$$

where $\boldsymbol{p}^T(x, y)=[p_1(\boldsymbol{x}), p_2(\boldsymbol{x}), \ldots, p_m(\boldsymbol{x})]$ is a vector of the complete monomial basis of order m. Examples of $\boldsymbol{p}^T(\boldsymbol{x})$ in a 2-D problem are:

$$\boldsymbol{p}^T(\boldsymbol{x})=\{1, x, y\} \text{ for linear basis, } m=3 \tag{9a}$$

$$\boldsymbol{p}^T(\boldsymbol{x})=\{1, x, y, x^2, xy, y^2\} \text{ for quadratic basis, } m=6 \tag{9b}$$

The m unknown coefficients $a_J(\boldsymbol{x}, t)$ are determined by minimizing a weighted discrete L_2 norm defined as:

$$J = \sum_{I=1}^{n} W(\boldsymbol{x}-\boldsymbol{x}_I)[\boldsymbol{p}^T(\boldsymbol{x}_I)\boldsymbol{a}(\boldsymbol{x}, t) - \hat{f}_I(t)]^2 \tag{10}$$

Here $\hat{f}_I$ is the fictitious value at time t of the function f at point $\boldsymbol{x}=\boldsymbol{x}_I$, and n is the number of points in the neighborhood of $\boldsymbol{x}$ for which the weight functions

$W(\boldsymbol{x}-\boldsymbol{x}_I)>0$. We choose the following fourth-order spline function to be the weight function:

$$W(\boldsymbol{x}-\boldsymbol{x}_I) = \begin{cases} 1-6\left(\frac{d_I}{r_I}\right)^2+8\left(\frac{d_I}{r_I}\right)^3-3\left(\frac{d_I}{r_I}\right)^4, & 0\le d_I\le r_I \\ 0, & d_I\ge r_I \end{cases} \tag{11}$$

where $d_I=|\boldsymbol{x}-\boldsymbol{x}_I|$ is the distance between points $\boldsymbol{x}$ and $\boldsymbol{x}_I$, and r_I is the radius of the circle outside of which $W(\boldsymbol{x}-\boldsymbol{x}_I)$ vanishes. r_I is called the support of the weight function.

Finding the extremum of $J(\boldsymbol{x})$ in Eq. (10) with respect to $\boldsymbol{a}(\boldsymbol{x}, t)$ leads to the following system of linear equation for the determination of $\boldsymbol{a}(\boldsymbol{x}, t)$:

$$\boldsymbol{A}(\boldsymbol{x})\boldsymbol{a}(\boldsymbol{x}, t) = \boldsymbol{B}(\boldsymbol{x})\hat{\boldsymbol{f}}(t) \tag{12}$$

where

$$\boldsymbol{A}(\boldsymbol{x}) = \sum_{I=1}^{n} W(\boldsymbol{x}-\boldsymbol{x}_I)\boldsymbol{p}(\boldsymbol{x}_I)\boldsymbol{p}^T(\boldsymbol{x}_I) \tag{13a}$$

$$\boldsymbol{B}(\boldsymbol{x})=[W(\boldsymbol{x}-\boldsymbol{x}_1)\boldsymbol{p}(\boldsymbol{x}_1),\ W(\boldsymbol{x}-\boldsymbol{x}_2)\boldsymbol{p}(\boldsymbol{x}_2),\ \cdots,\ W(\boldsymbol{x}-\boldsymbol{x}_n)\boldsymbol{p}(\boldsymbol{x}_n)] \tag{13b}$$

Solving $\boldsymbol{a}(\boldsymbol{x}, t)$ from Eq. (12) and substituting it into Eq. (8), we have the following relation for nodal interpolation

$$f^h(\boldsymbol{x}, t) = \sum_{I=1}^{n} \phi_I(\boldsymbol{x})\hat{f}_I(t) \tag{14}$$

where

$$\phi_I(\boldsymbol{x}) = \sum_{J=1}^{m} p_J(\boldsymbol{x})[\boldsymbol{A}^{-1}(\boldsymbol{x})\boldsymbol{B}(\boldsymbol{x})]_{JI} \tag{15}$$

$\phi_I(x)$ is usually called the basis function of the MLS approximation corresponding to node I. Note that $\phi_I(\boldsymbol{x}_J)$ need not equal the Kronecker delta δ_{IJ}, and thus $\hat{f}_I(t)\neq f^h(\boldsymbol{x}_I, t)$. For the matrix $\boldsymbol{A}$ to be invertible, the number of n points must at least equal m (e.g. $n\ge m$). For m=3 or 6, Chati and Mukherjee (2000) have suggested that $15\le n\le 30$ give acceptable results for 2-D elastostatic problems. For an elastodynamic problem, Batra and Ching (2002) used Gauss weight functions, m=6 and r_I=3.5 times the distance between the point $\boldsymbol{x}_I$ and the third node nearest to the node at $\boldsymbol{x}_I$. In this paper, we take

$$r_I=bh_I \tag{16}$$

where h_I is the distance from node I to its nearest neighbor, and b is a scaling parameter. The choice of the parameter b does affect the computed results, and we will elaborate it in section IV.

2. General Semidiscrete Formulation

We assume that N nodes are placed on Ω, and $S_1, S_2, \cdots, S_N$ are smooth 2-D closed regions, not necessarily disjoint and of the same shape. Here, each of the regions is conveniently taken to be a circle centered at $\boldsymbol{x}_I$ with the radius equal to h_I (I=1, 2, ⋯, N). For one of these regions, say S_α, let $\phi_1, \phi_2, \cdots, \phi_n$ and $\psi_1, \psi_2, \cdots, \psi_n$ be linearly independent functions defined on it. The unknown trial function $\boldsymbol{u}$ and the test function $\tilde{\boldsymbol{u}}$ can be written respectively by

$$\boldsymbol{u} = \begin{Bmatrix} u(\boldsymbol{x}, t) \\ v(\boldsymbol{x}, t) \end{Bmatrix} = \sum_{J=1}^{n} \phi_J\boldsymbol{\delta}_J(t) \tag{17a}$$

$$\tilde{\boldsymbol{u}} = \begin{Bmatrix} \tilde{u}(\boldsymbol{x}) \\ \tilde{v}(\boldsymbol{x}) \end{Bmatrix} = \sum_{I=1}^{n} \psi_I\tilde{\boldsymbol{\delta}}_I \tag{17b}$$

where $\boldsymbol{\phi}_J=\phi_J\boldsymbol{I}$ and $\boldsymbol{\psi}_I=\psi_I\boldsymbol{I}$; $\boldsymbol{I}$ is a 2×2 identity matrix. $\boldsymbol{\delta}_J$ and $\tilde{\boldsymbol{\delta}}_I$ are 2×1 arrays. Note that $\boldsymbol{\delta}_J$ are functions of time t. Substitution of Eqs. (17a) and (17b) into (7) gives

$$\boldsymbol{\varepsilon} = \sum_{J=1}^{n} \boldsymbol{B}_J\boldsymbol{\delta}_J, \quad \tilde{\boldsymbol{\varepsilon}} = \sum_{I=1}^{n} \tilde{\boldsymbol{B}}_I\tilde{\boldsymbol{\delta}}_I \tag{18a,b}$$

where

$$\boldsymbol{B}_J = \begin{bmatrix} \frac{\partial\phi_J}{\partial x} & 0 \\ 0 & \frac{\partial\phi_J}{\partial y} \\ \frac{\partial\phi_J}{\partial y} & \frac{\partial\phi_J}{\partial x} \end{bmatrix}, \quad \tilde{\boldsymbol{B}}_I = \begin{bmatrix} \frac{\partial\psi_I}{\partial x} & 0 \\ 0 & \frac{\partial\psi_I}{\partial y} \\ \frac{\partial\psi_I}{\partial y} & \frac{\partial\psi_I}{\partial x} \end{bmatrix} \tag{19a,b}$$

Replacing the domain Ω of integration in Eq. (4) by S_α, substituting for $\boldsymbol{u}$, $\tilde{\boldsymbol{u}}$, $\boldsymbol{\varepsilon}$, and $\tilde{\boldsymbol{\varepsilon}}$ from Eqs. (17) and (18) for each region, and requiring that the resulting equations hold for all choices of $\tilde{\boldsymbol{\delta}}$, we arrive at the following system of coupled ordinary differential equations:

$$\sum_{J=1}^{N} \boldsymbol{M}_{IJ}\ddot{\boldsymbol{\delta}}_J + \boldsymbol{K}_{IJ}\boldsymbol{\delta}_J = \boldsymbol{F}_I, \quad I=1, 2, 3, \cdots, N \tag{20}$$

Here

$$\boldsymbol{M}_{IJ} = \int_{S_\alpha} \rho\psi_I^T\phi_J d\Omega \tag{21a}$$

$$\boldsymbol{K}_{IJ} = \int_{S_\alpha} \tilde{\boldsymbol{B}}_I^T\boldsymbol{D}\boldsymbol{B}_J d\Omega - \int_{\Gamma_{\alpha u}} \psi_I^T\boldsymbol{N}\boldsymbol{D}\boldsymbol{B}_J d\Gamma - \int_{\Gamma_{\alpha 0}} \psi_I^T\boldsymbol{N}\boldsymbol{D}\boldsymbol{B}_J d\Gamma \tag{21b}$$

$$\boldsymbol{F}_I = \int_{\Gamma_{\alpha t}} \psi_I^T \overline{\boldsymbol{t}}\, d\Omega \tag{21c}$$

where $\Gamma_{\alpha 0}=\partial S_\alpha-\Gamma_{\alpha u}-\Gamma_{\alpha t}$, $\Gamma_{\alpha u}=\partial S_\alpha\cap\Gamma_u$, and $\Gamma_{\alpha t}=\partial S_\alpha\cap\Gamma_t$. $\boldsymbol{M}_{IJ}$, $\boldsymbol{K}_{IJ}$, and $\boldsymbol{F}_I$ are usually called the stiffness matrix, the mass matrix and the load vector respectively. In the MLPG formulation, $\boldsymbol{K}_{IJ}$ and $\boldsymbol{M}_{IJ}$ need not be symmetric.

Various options of the test function leading to different MLPG formulations have been provided by Atluri and Shen (2002). By making the test function $\psi_I(\boldsymbol{x})$ equal to the weight function $W(\boldsymbol{x}-\boldsymbol{x}_I)$ of the moving least squares approximation with $r_I=h_I$, the integrals on $\Gamma_{\alpha 0}$ identically vanish, and henceforth evaluation of the stiffness matrix can be simplified. A numerical integration is required to evaluate the domain integral on S_α and the line integral on ∂S_α in Eq. (21). The region S_α, and the boundary $\Gamma_{\alpha u}$ and $\Gamma_{\alpha t}$ on ∂S_α are mapped onto a $[-1,1]\times[-1,1]$ square domain and a $[-1,1]$ straight line, respectively, and the Gauss quadrature rule is utilized to numerically evaluate these integrals. Therefore, the MLPG method is a "truly meshless" scheme because no shadow cells need to be established for the purpose of integration.

In order to derive initial conditions on $\boldsymbol{\delta}_J$, we substitute Eq. (17a) into Eq. (2a), multiply both sides of the resulting equation by $\rho\tilde{\boldsymbol{u}}$ from Eq. (17b), integrate it over S_α and exploit the fact that it must hold for all choices of $\tilde{\boldsymbol{\delta}}_I$; a similar procedure is also applied to find $\dot{\boldsymbol{\delta}}_J$. We have $\boldsymbol{\delta}_I$ and $\dot{\boldsymbol{\delta}}_J$ for

$$\boldsymbol{M}_{IJ}\boldsymbol{\delta}_J(0) = \int_{S_\alpha} \rho\psi_I^T \boldsymbol{u}^0(\boldsymbol{x})dS \tag{22a}$$

$$\boldsymbol{M}_{IJ}\dot{\boldsymbol{\delta}}_J(0) = \int_{S_\alpha} \rho\psi_I^T \dot{\boldsymbol{u}}^0(\boldsymbol{x})dS \tag{22b}$$

Eq. (20) can be simplified by setting $\ddot{\boldsymbol{\delta}}_J=0$ for the static analysis. For a free vibration analysis, the loading vector $\boldsymbol{F}_I=0$, $\boldsymbol{\delta}_J(t)$ can be written as

$$\boldsymbol{\delta}_J(t) = e^{i\omega t}\overline{\boldsymbol{\delta}}_J \tag{23}$$

Substituting Eq. (23) into Eq. (20) leads to the following eigenvalue equation

$$\boldsymbol{K}_{IJ}\overline{\boldsymbol{\delta}}_J = \omega^2\boldsymbol{M}_{IJ}\overline{\boldsymbol{\delta}}_J \tag{24}$$

The natural frequency ω and its corresponding eigenmode $\overline{\boldsymbol{\delta}}_J$ can be obtained by solving Eq. (24).

3. Estimation of Effective Elastic Constants in FGMs

Analytical functions such as the exponent and power-law functions are commonly used in describing the continuously varying material properties in FGMs because these functions facilitate obtaining exact solutions in the analysis of FG structures. In terms of local compositions of material constituents, however, this approach based on the continuum models may not physically determine the variation of material properties in FGMs. Another approach used to characterize the material gradation and infer the effective material properties is based on the micromechanical models among which the Hashin-Shtrikman bounds (Hashin and Shtrikman, 1963), the self-consistent method (Hill, 1965), the Mori-Tanaka method (Mori and Tanaka, 1973), and the mean field approach (Wakashima and Tsukamoto, 1991) are popular schemes. Although the local effective material properties of FGMs can also be estimated by the rule of mixtures, this method does not account for the interaction between phases and thus it only gives very approximate values of the effective elastic moduli. On the other hand, the micromechanical approach takes account of the interactions and uses a certain representative volume element (RVE) to estimate the average local stress and strain fields of the constituents of the composite. Then, the local average fields are used to evaluate the effective material properties. Vel and Batra (2002) have used both the Mori-Tanaka and the self-consistent methods to find an analytical solution for thermoelastic deformations of a simply supported FG plate. Compared with the self-consistent method, it is easier to use the Mori-Tanaka method because the self-consistent method requires solving for a quartic equation to obtain the shear modulus.

In this paper, we adopt the Mori-Tanaka method to estimate the effective material moduli at a point in FGM. The Mori-Tnanka method is derived for regions of the graded microstructure that have a well-defined continuous matrix and a discontinuous particle phase. The method has been found to have the same expressions as the Hashin-Shtrikman lower bound bounds when the inclusions are spherical. For a two-phase composite, we summarize the Mori-Tanaka method in the following. It is assumed that the matrix phase, denoted by the subscript 1, is reinforced by spherical particles of a particulate phase, denoted by the subscript 2. The local effective bulk modulus K and the shear modulus G are given by

$$\frac{K-K_1}{K_2-K_1} = \frac{V_2}{1+3(1-V_2)(K_2-K_1)/(3K_1+4G_1)} \tag{25}$$

$$\frac{G-G_1}{G_2-G_1} = \frac{V_2}{1+(1-V_2)(G_2-G_1)/(G_1+f_1)} \tag{26}$$

where $f_1=G_1(9K_1+8G_1)/6(K_1+2G_1)$. K_1 and G_1 are the

bulk modulus and the shear modulus, respectively, and V_1 the volume fraction of the matrix phase. K_2, G_2 and V_2 denote the corresponding material properties and the volume fraction of the particulate phase. It should be noted that $V_1+V_2=1$, and the Young's modulus and the Poisson's ratio are related to the bulk and shear moduli by $E=9KG/(3K+G)$ and $\nu=(3K-2G)/2(3K+G)$, respectively.

The mass density ρ at a point is obtained by the "rule of mixtures":

$$\rho=\rho_1 V_1+\rho_2 V_2 \tag{27}$$

where ρ_1 and ρ_2 are the densities of matrix and particulate phases, respectively.

4. Imposition of Essential Boundary Conditions

In the MLPG method, the lack of the Kronecker delta property of the basis function $\phi_i(x)$ poses difficulty in satisfying the essential boundary conditions. Several techniques such as the penalty method (e.g. see Atluri and Zhu, 1998), the orthogonal transformation method (e.g. see Atluri and Shen, 2002), the singular value decomposition (SVD) method (e.g. see Gu and Liu, 2001a) and the Lagrange multiplier method have been proposed to overcome the above problem. Among these methods, the penalty method is easiest to use. Whereas the penalty method provides a simple approach to impose essential boundary conditions, the selection of the penalty parameter remains a challenge (Belytschko *et al*., 2000). For instance, Qian *et al*. (2003a) found that the value of the penalty parameter affects, noticeably, the computed results when the MLPG method is used to analyze a thick plate with a higher-order shear and normal deformable theory. Batra and Ching (2002) also found that the time used to compute a stable solution for a transient elastodynamic problem by the explicit central-difference method also depends on the value assigned to the penalty parameter. As compared to the penalty method, the orthogonal transformation technique exactly satisfies the essential boundary conditions, and also eliminates the prescribed degrees of freedom in Eq. (20) so that the size of the system of equations is reduced. The singular decomposition method can be regarded as a special case of the orthogonal transformation technique. However, the method can only be applied to a problem in which the essential boundary conditions are homogeneous. The Lagrange multiplier method has been commonly used to impose constraint equations in the finite element method, but this method increases the number of degrees of freedom and yields a non-positive definite system matrix. In view of both advantages and shortcomings for the above schemes, we apply the orthogonal transformation technique to impose the boundary conditions in our study.

Let D and I denote respectively the set of degrees of freedom where displacements are and are not prescribed. The displacement $\boldsymbol{u}$ can be written as

$$\boldsymbol{u}=\begin{Bmatrix}\boldsymbol{u}^D\\ \boldsymbol{u}^I\end{Bmatrix}=\begin{bmatrix}\phi^{DD} & \phi^{DI}\\ \phi^{ID} & \phi^{II}\end{bmatrix}\begin{Bmatrix}\boldsymbol{\delta}^D\\ \boldsymbol{\delta}^I\end{Bmatrix} \tag{28}$$

Solving the first of these equations for $\boldsymbol{\delta}^D$, we get

$$\boldsymbol{\delta}=\begin{Bmatrix}\boldsymbol{\delta}^D\\ \boldsymbol{\delta}^I\end{Bmatrix}=\begin{Bmatrix}(\phi^{DD})^{-1}\boldsymbol{u}^D\\ \boldsymbol{0}\end{Bmatrix}+\begin{bmatrix}-(\phi^{DD})^{-1}\phi^{DI}\\ \boldsymbol{I}\end{bmatrix}\boldsymbol{\delta}^I \tag{29}$$

where $\boldsymbol{0}$ and $\boldsymbol{I}$ are null and the identity matrices respectively. Substitution from Eq. (30) into Eq. (20) and the premultiplication of the resulting equation by $\begin{bmatrix}-(\psi^{DD})^{-1}\psi^{DI}\\ \boldsymbol{I}\end{bmatrix}^T$ give

$$\overline{\boldsymbol{M}}\,\ddot{\boldsymbol{\delta}}^I+\overline{\boldsymbol{K}}\,\boldsymbol{\delta}^I=\overline{\boldsymbol{F}} \tag{30}$$

where

$$\overline{\boldsymbol{M}}=\begin{bmatrix}-(\psi^{DD})^{-1}\psi^{DI}\\ \boldsymbol{I}\end{bmatrix}^T\boldsymbol{M}\begin{bmatrix}-(\phi^{DD})^{-1}\phi^{DI}\\ \boldsymbol{I}\end{bmatrix} \tag{31a}$$

$$\overline{\boldsymbol{K}}=\begin{bmatrix}-(\psi^{DD})^{-1}\psi^{DI}\\ \boldsymbol{I}\end{bmatrix}^T\boldsymbol{K}\begin{bmatrix}-(\phi^{DD})^{-1}\phi^{DI}\\ \boldsymbol{I}\end{bmatrix} \tag{31b}$$

$$\overline{\boldsymbol{F}}=\begin{bmatrix}-(\psi^{DD})^{-1}\psi^{DI}\\ \boldsymbol{I}\end{bmatrix}^T\boldsymbol{F}+\begin{bmatrix}-(\psi^{DD})^{-1}\psi^{DI}\\ \boldsymbol{I}\end{bmatrix}^T\cdot\boldsymbol{K}\begin{Bmatrix}(\phi^{DD})^{-1}\boldsymbol{u}^D\\ \boldsymbol{0}\end{Bmatrix} \tag{31c}$$

5. The Time Integration Scheme

We use the Newmark family of methods (Newmark, 1959) to integrate Eq. (30). The recursive relations for displacements, velocities and accelerations between time t_n and t_{n+1} are

$$\boldsymbol{\delta}^J_{n+1}=\boldsymbol{\delta}^J_n+\Delta t\dot{\boldsymbol{\delta}}^J_n+\frac{(\Delta t)^2}{2}\{(1-2\beta)\ddot{\boldsymbol{\delta}}^J_n+2\beta\ddot{\boldsymbol{\delta}}^J_{n+1}\} \tag{32a}$$

$$\dot{\boldsymbol{\delta}}^J_{n+1}=\dot{\boldsymbol{\delta}}^J_n+\Delta t\{(1-\gamma)\ddot{\boldsymbol{\delta}}^J_n+\gamma\ddot{\boldsymbol{\delta}}^J_{n+1}\} \tag{32b}$$

$$\ddot{\boldsymbol{\delta}}^J_{n+1}=\frac{1}{\beta(\Delta t)^2}\{\boldsymbol{\delta}^J_{n+1}-\boldsymbol{\delta}^J_n\}-\frac{1}{\beta(\Delta t)}\dot{\boldsymbol{\delta}}^J_n-\frac{1}{2\beta}\ddot{\boldsymbol{\delta}}^J_n \tag{32c}$$

where $\boldsymbol{\delta}_n^J$, $\dot{\boldsymbol{\delta}}_n^J$, and $\ddot{\boldsymbol{\delta}}_n^J$ denote the displacements, velocities and accelerations, respectively, at time $t_n=n\Delta t$ and Δt is the uniform time interval between two time steps. β and γ are the parameters that control the stability and the accuracy of the time integration scheme. The Newmark family of methods is unconditionally stable if

$$\gamma \geq \frac{1}{2} \text{ and } \beta \geq \frac{1}{4}(\frac{1}{2}+\gamma) \tag{33}$$

The methods are second-order accurate and nondissipative for γ=1/2 and first-order accurate and dissipative for γ≠1/2.

IV. RESULTS AND DISCUSSION

A computer code based on the aforestated equations is developed and used to analyze a cantilever beam made of a two-phase steel/aluminum FG composite and subjected to a normal traction $q(x, t)$ on the top surface. A schematic sketch of the problem is depicted in Fig. 1(a). Here we take length L=200 mm, thickness h=20 mm, and width w=5 mm. As $w<<L$, a plane stress state is assumed to prevail in the beam. A regular nodal mesh (see Fig. 1(b)) of 729 nodes with 81 and 9 equally spaced in the longitudinal and thickness directions respectively is used. We use 9×9 and 9 quadrature points to numerically evaluate the respective domain and boundary integrals appearing in Eq. (21), and set m=3 for the linear basis. Material properties of the steel and aluminum (*Al*) are:

Steel: E_s=210GPa, v_s=0.29, ρ_s=7806 kg/m^3

Al: E_a=70GPa, v_a=0.3, ρ_a=2707 kg/m^3

Here E is the Young's modulus and v the Poisson ratio. We assume that steel corresponds to constituent 1 and aluminum to 2 in Eqs. (25), (26) and (27). The volume fraction of the aluminum phase is assumed to vary in both longitudinal and thickness directions by a power-law-type function as

$$V_{Al} = (\frac{y}{h})^p(\frac{x}{L})^q,\ 0\leq p<\infty,\ 0\leq q<\infty \tag{34}$$

where p and q are parameters that dictate the volume fraction profile through the domain of the beam. The increase of p and q indicate that the beam is enriched with more steel. For example, the FG beam with p=q=0 corresponds to a pure aluminum beam, while $p, q\to\infty$ to a pure steel beam. With Eq. (34), variations of Young's modulus and mass density for p=0 and various values of q along the longitudinal direction can be plotted in Figs. 2(a) and 2(b), respectively. The material properties in these two figures are normalized to those of steel respectively. It is shown

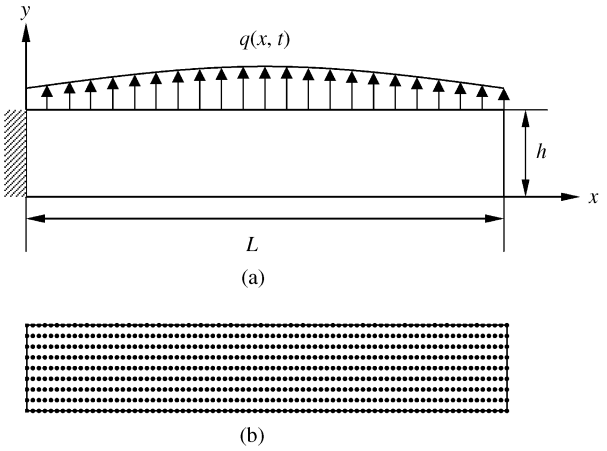

Fig. 1 (a) A schematic sketch of a cantilever beam subjected to a normal traction; (b) a uniform nodal mesh of 729 nodes

that the material properties vary from those of steel at the fixed end to those of aluminum at the free end.

Finite element (FE) analyses are performed to validate the present numerical solutions. We used eight-node quadrilateral elements. Each element was modeled as a homogeneous solid wherein its material properties were assigned according to the material gradation of the FG beam at its centroid. In the tables and figures to follow, vertical deflection or transverse displacement v and natural frequency ω are non-dimensionalized by

$$\overline{v} = \frac{10E_s h^3}{12L^4(1-v_s^2)q_0}v,\ \ \overline{\omega} = 10\omega h\sqrt{\rho_s/E_s} \tag{35a,b}$$

Here q_0 is the intensity of the normal traction q, and an overbar signifies a non-dimensional quantity.

The size of the support, r_I, of the weight function is decided by the scaling parameter b in Eq. (16). A very small r_I will result in a relatively large numerical error in the accuracy of computed solutions (Atluri and Zhu, 2000). On the other hand, r_I should also be small enough to preserve the local character of the MLPG formulations. To chose a proper value of the parameter b, we conduct a convergence study of b on the vertical deflections at x=L, y=h/2 for FG beams with p=0, q=2 and p=0, q=5, respectively. Results plotted in Fig. 3 for b with a wide range of value from 2 to 15 reveal that that b≥5 leads to convergent solutions, and henceforth we choose b=7 in the following analyses

1. Static Analysis

In the static analysis, we consider an FG beam loaded by a uniformly normal traction q_0 on the top surface. Fig. 4 shows the non-dimensional vertical deflections $\overline{v}$ at y=h/2 along the span with the volume fraction varying in the longitudinal direction

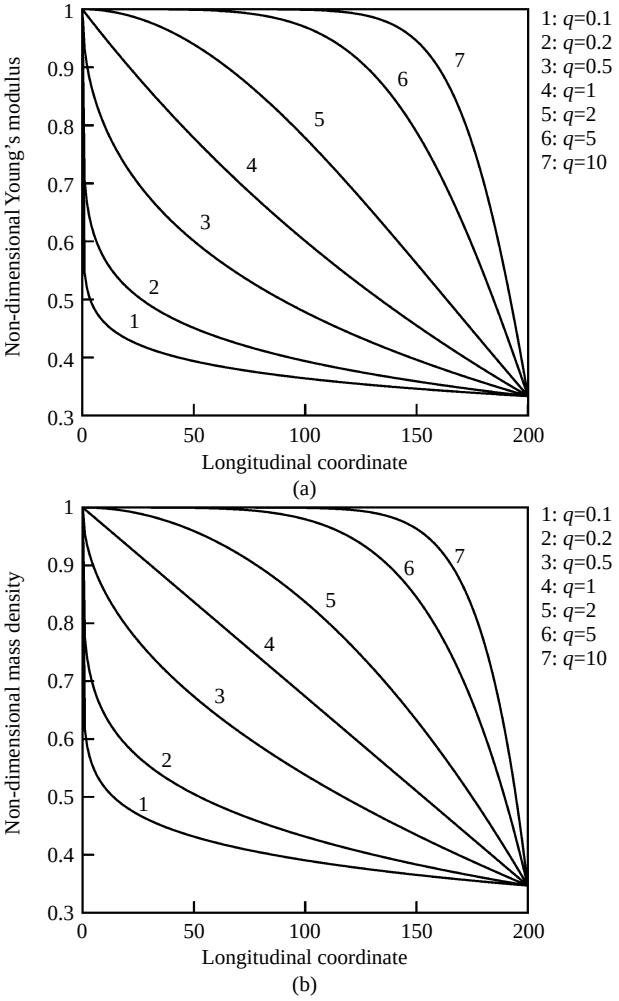

Fig. 2 (a) The profiles of non-dimensional Young's modulus along the longitudinal direction of FG beams for p=0 and different values of q; (b) the profiles of non-dimensional mass density along the longitudinal direction of FG beams for p=0 and different values of q

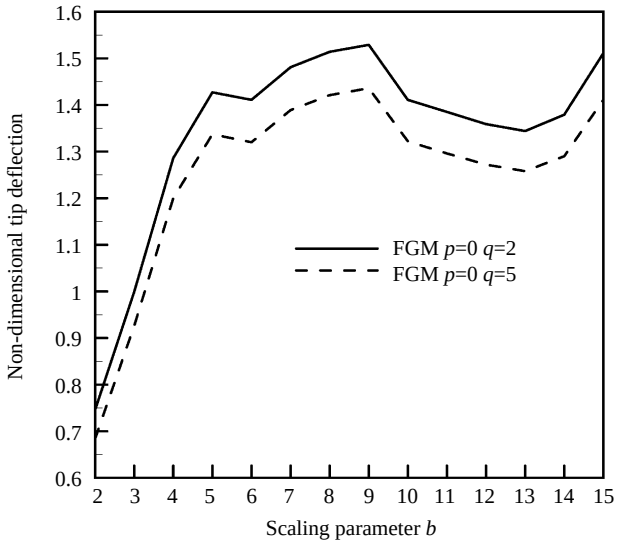

Fig. 3 Convergence of non-dimensional tip deflections at $y=h/2$ with the value of the scaling parameter b

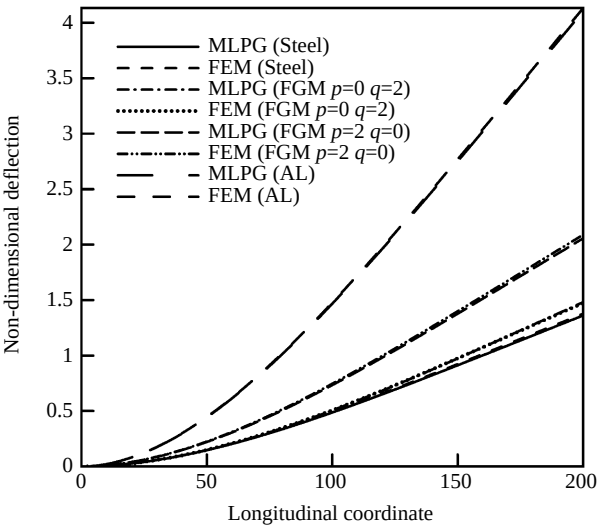

Fig. 4 Variations of non-dimensional deflections computed by the MLPG method and FEM at $y=h/2$ along the longitudinal direction of the beam

(i.e. p=0, q=2) and the thickness direction (i.e. p=2, q=0). The deflections computed for both the steel beam and aluminum beam are also included. The MLPG results are in good agreement with their corresponding FE solutions. It is noted that, from the homogeneous beam theory, the deflection of the cantilever beam (i.e. $v=q_0L^4/8EI$) is inversely proportional to the Young's modulus E for a given loading and geometry configuration. For the present FG beam, the Young's modulus of the steel gradually varies either from the fixed to the free end or from the bottom to the top surface until the aluminum is fully enriched. As expected in Fig. 4 the deflections of FG beams fall in between those of their homogeneous counterparts. The non-dimensional vertical deflections along the longitudinal direction with p=2 and different values of q are exhibited in Fig. 5. It shows that the increase of the index q produces a decrease of deflections. We further evince the tip deflections, as shown in Fig. 6, at $x=L$, $y=h/2$ with the power-law index q for different values of p. The largest value of p gives the minimum tip deflection and vice versa. For a given index p, the tip deflections change rapidly for small values of q, and stay almost the same for large values of q.

2. Free Vibration Analysis

Gu and Liu (2001a) have applied the MLPG method to analyze the free vibration of a cantilever beam made of homogeneous materials. The results of eigenmodes and natural frequencies compared well with those obtained from the FEM. For an FG

Table 1 Comparison of non-dimensional natural frequencies from the FEM with the MLPG method

Mode	Steel		FGMs (p=0, q=2)		*AL*	
	FEM	MLPG	FEM	MLPG	FEM	MLPG
1	0.1008	0.1020	0.1306	0.1313	0.0989	0.0997
2	0.6050	0.5951	0.6490	0.6396	0.5932	0.5840
3*	1.5725	1.5709	1.6084	1.5903	1.5420	1.5402
4	1.5940	1.5758	1.8326	1.8315	1.5627	1.5448
5	2.8976	2.8678	2.8713	2.8425	2.8400	2.8102
6	4.4202	4.3805	4.3453	4.3068	4.3314	4.2909
7*	4.7144	4.7103	4.7347	4.7311	4.6225	4.6182
8	6.0870	6.0374	5.9589	5.9109	5.9638	5.9122
9*	7.8460	7.7893	7.6643	7.6074	7.6887	7.6261
10	7.8483	7.8395	7.7131	7.7074	7.6924	7.6854

Note: The mode number denoted by a* indicates an axial vibration, but otherwise is a bending vibration

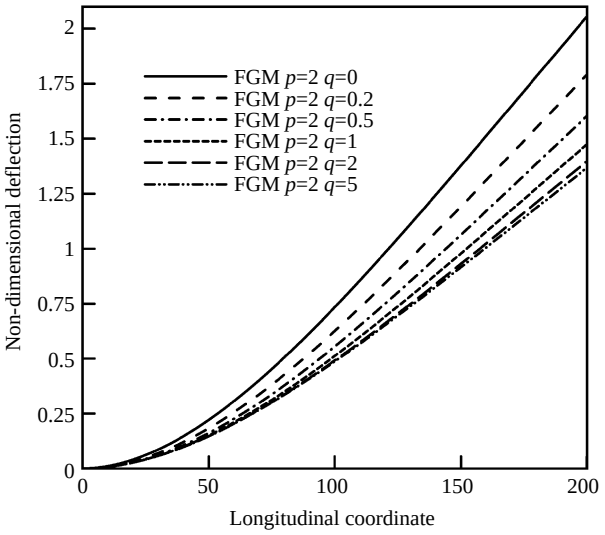

Fig. 5 Variations of non-dimensional deflections at $y=h/2$ along the lonitudinal direction of FG beams for p=2 and different values of q

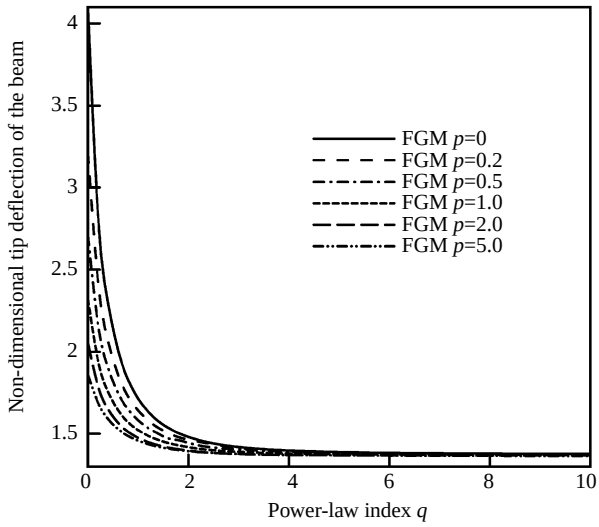

Fig. 6 Variations of non-dimensional tip deflections of FG beams with the power-low index q for different values of p

cantilever beam, free vibration analyses using the MLPG method are presented here. Table 1 lists the first ten non-dimensional natural frequencies for an FG beam with p=0 and q=2 as well as for both steel and aluminum beams. Excellent agreements are obtained as compared with the FE solutions. We also investigate the eigenmodes for various values of p and q. The mode shapes of an FG beam are found to be independent of indices p and q, and the same as those of a homogeneous beam. Thus, the plots of the eigenmodes are omitted so as not to repeat the results as reported in Gu and Liu (2001a). Table 2 gives the MLPG results of the first ten non-dimensional frequencies for different values of p and q. It can be seen that the maximum first frequency occurs at p=0 and q=1.23. This conclusion is more evident in Fig. 7 which shows variations of the first frequency with q for p=0, 2 and 5 respectively. We see from Fig. 7, Tables 1 and 2 that the first frequency of the FG beam with p=0 and q=1.23, reaching $\overline{\omega}_1$=0.1335, is 34% and 32.3% higher than those of the aluminum and steel beam respectively. It can be seen from Table 2 that the second and thereafter frequencies corresponding to p=0 and q=1.23 are not the maximum among different values of p and q. p=0 and q=4.70 are the values for the second maximum bending frequency of $\overline{\omega}_2$=0.6465, which is 10.76% and 6.85% higher than those of corresponding aluminum and steel beams. This conclusion can also be shown in Fig. 8.

3. Forced Vibration Analysis

For both the MLPG and FE solutions in the forced vibration analysis, we take γ=1/2 and β=1/4

Table 2 Non-dimensional natural frequencies of FG beams with the power-law indices p and q

Mode	p=0					p=2			p=4		
	q=0	q=1.23	q=2	q=4	q=4.7	q=0	q=2	q=4	q=0	q=2	q=4
1	0.0997	0.1335	0.1313	0.1230	0.1209	0.0939	0.1091	0.1078	0.0931	0.1059	0.1054
2	0.5840	0.6337	0.6396	0.6465	0.6465	0.5490	0.5990	0.6056	0.5545	0.5935	0.5999
3*	1.5402	1.5733	1.5903	1.6242	1.6315	1.4634	1.5543	1.5758	1.4756	1.5508	1.5697
4	1.5448	1.8448	1.8315	1.7620	1.7429	1.5287	1.6377	1.6259	1.5453	1.6095	1.6030
5	2.8102	2.8140	2.8425	2.8982	2.9109	2.6810	2.8185	2.8528	2.7046	2.8191	2.8483
6	4.2909	4.2658	4.3068	4.3828	4.4001	4.1199	4.3022	4.3483	4.1601	4.3089	4.3471
7*	4.6182	4.6751	4.7311	4.8537	4.8778	4.5843	4.6799	4.7274	4.6343	4.6904	4.7182
8	5.9122	5.8565	5.9109	6.0071	6.0288	5.7078	5.9313	5.9883	5.7691	5.9463	5.9918
9*	7.6261	7.5389	7.6074	7.7240	7.7502	7.3971	7.6568	7.7239	7.4835	7.6820	7.7332
10	7.6854	7.6262	7.7074	7.8618	7.8963	7.6304	7.7573	7.8113	7.7140	7.7901	7.8213

Note: The mode number denoted by a* indicates an axial vibration, otherwise is a bending vibration

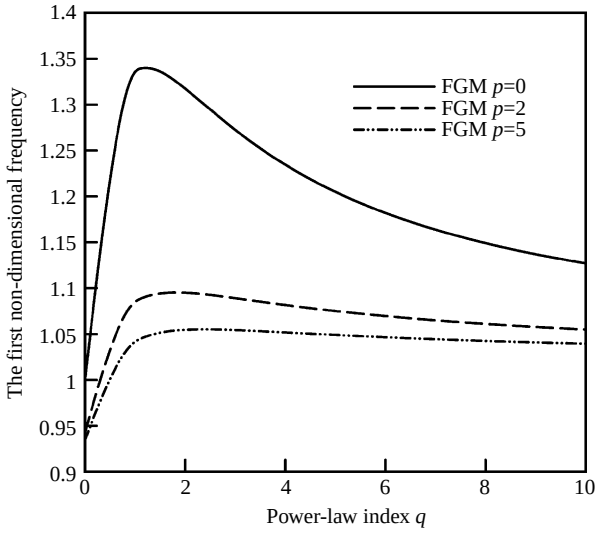

Fig. 7 Variations of the first non-dimensional frequencies of FG beams with the power-law index q for p=0, 2 and 5 respectively; frequencies are normalized with respect to that of the FG beam with p=0, q=0

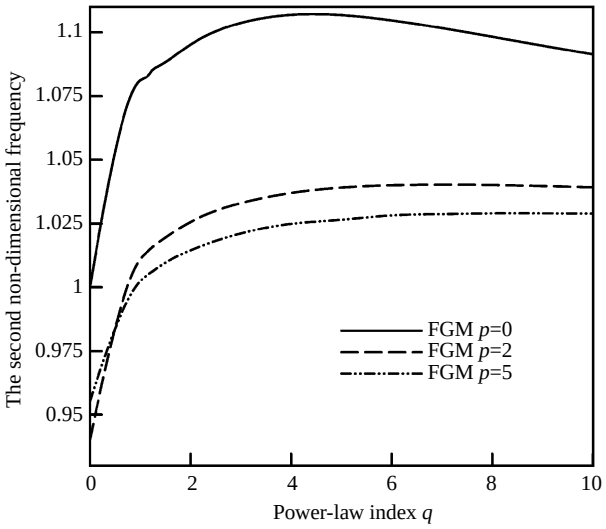

Fig. 8 Variations of the second non-dimensional frequencies of FG beams with the power-law index q for p=0, 2 and 5 respectively; frequencies are normalized with respect to that of the FG beam with p=0, q=0

in the Newmark family of methods. This time integration scheme, also known as the average acceleration method, is unconditionally stable and we set time step Δt equal to 2.5×10^{-4} sec. First, consider a uniformly harmonic normal load $q_0 \sin(\omega_f t)$ applied on the top surface of the beam for a period of 50 ms; ω_f is the driving frequency and taken ω_f=300 rad/sec. Figs. 9 and 10 depict the time histories of tip deflections at $x=L$, $y=h/2$ for a steel beam and an FG beam with p=0, q=2 respectively. It can be found in each figure that the time histories of the deflections obtained by the MLPG method and the FEM match very well, and the responses excited by the driving frequency ω_f are steadily oscillated with the same amplitudes. In Fig. 11, we compare the time histories of the tip deflections for p=0 and different values of q. The harmonic responses depend on the power-law indices p and q, the amplitudes of tip deflections decrease with the increase of the index q. Next, a uniformly normal traction with Heavside time dependence (i.e. $q=q_0H(t)$) is considered. The time histories of tip deflections for an FG beam with p=0, q=2 are displayed in Fig. 12. The loading is first applied on the beam and subsequently released after 10 ms. Results obtained by the MLPG method agree well with those obtained by the FEM for duration of both forced and free vibrations. One of the appealing properties of FGMs can be illustrated in Fig. 13, where the time histories of tip deflections of the steel beam and FG beams are plotted. One can observe that the response of the FG beam with p=0, q=4.7 during the period of forced vibration (within 25 ms) is of the

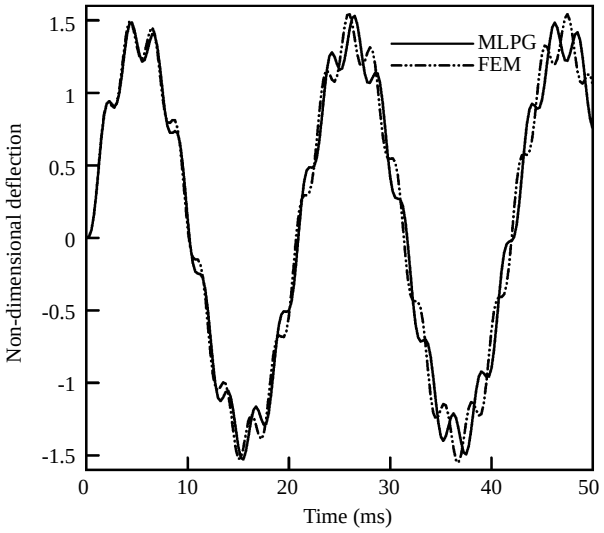

Fig. 9 Time histories of tip deflections of a steel beam under a uniformaly harmonic normal traction of $q_0 \sin(300t)$

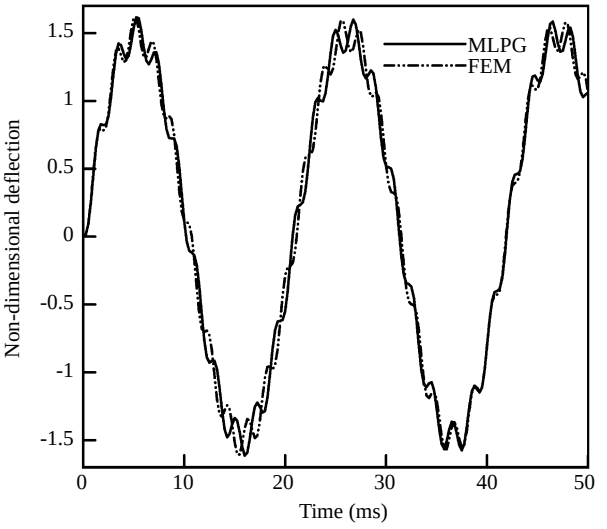

Fig. 10 Time histories of tip deflections of an FG beam with p=0, q=2 under a uniformly harmonic normal traction of q_0 sin (300t)

same amplitude as that of the steel beam whereas the response of the FG beam with p=0 and q=1.23 gives larger amplitudes than those of the steel and the FG beam with p=0 and q=4.7. Meanwhile, one can also observe that the the FG beam with p=0 and q=4.7 gives the minimum amplitudes among these three kinds of beams during the period of free vibration after 25 ms. It is clear that the dynamic response of FGMs such as the amplitudes of deflection can be diminished by suitably adjusting the volume fraction of the constituents.

V. CONCLUSIONS

MLPG solutions for static deformations, free vibrations and forced vibrations of an FG cantilever beam have been presented in this paper. The FG beam is made of a two-phase steel/aluminum composite wherein the effective material moduli at a point are determined by the Mori-Tanaka method. The MLPG method gives results very close to those obtained from the FEM in each analysis. Static analysis shows that the deflections of FG beams are bounded from above by that of an aluminum beam and from below by that of a steel beam. In the free vibration analysis, however, we found that the maximum first frequency occurs in an FG beam with p=0, q=1.23 rather than in a homogeneous beam. Computed results show that

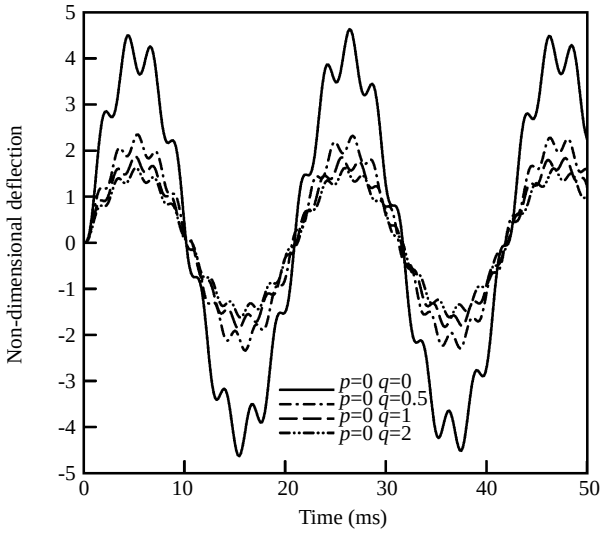

Fig. 11 Time histories of tip deflections of an FG beams with p=0 and different values of q under a uniformly harmonic normal traciton of $q_0 \sin(300t)$

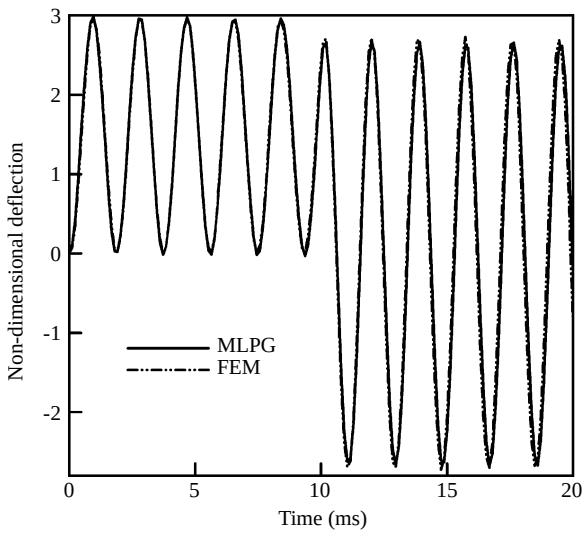

Fig. 12 Time histories of tip deflections of an FG beams with p=0, q=2 under a step normal traction of q_0 for 10 ms

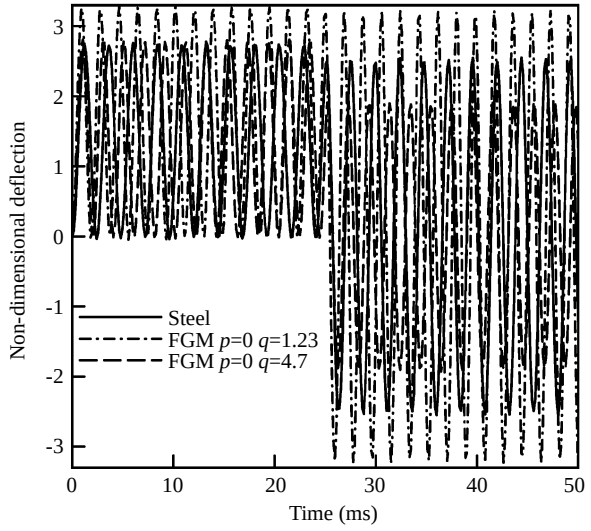

Fig. 13 Time histories of tip deflections for a steel beam, and FG beams with p=0, q=1.23 and p=0, q=4.7 under a step normal traction of q_0 for 25 ms

the maximum first frequency of this FG beam is 34% and 32.3% higher than those of the aluminum and steel beam respectively. The response of an FG beam subjected to forced vibration depends on the power-law indices p and q. By appropriately tailoring the volume fractions of constituents in an FG beam, the amplitudes of deflections can be minimized as compared to its homogeneous counterparts.

Through a series of examples, the MLPG method has been proven to be effective in the present investigations. The MLPG method is a truly meshless scheme, which requires only a set of nodes for both interpolation and integration. Furthermore, the method dictates the continuous material properties of FGMs directly to a quadrature point without formulations being modified. As a result, the prominent features of the MLPG method make it easy to implement in the analysis of functionally graded structures.

ACKNOWLEDGMENTS

The authors would like to thank Professor R. C. Batra at Virginia Tech. for his encouragement and guidance on this work. L. F. Qian and H. K. Ching would also like to acknowledge the support from the China Scholarship Council and Materials Technology Center at Southern Illinois University, respectively.

REFERENCES

Atluri, S. N., Kim, H. G., and Cho, J. Y., 1999, "A Critical Assessment of the Truly Meshless Local Petrov-Galerkin (MLPG) and Local Boundary Integral Equation (LBIE) Methods," *Computational Mechanics*, Vol. 24, No. 5, pp. 348-372.

Atluri, S. N., and Shen, S. P., 2002, *The Meshless Local Petrov-Galerkin (MLPG) Method*, Tech. Science Press, Los Angeles, USA.

Atluri, S. N., and Zhu, T., 1998, "A New Meshless Local Petrov-Galerkin (MLPG) Approach in Computational Mechanics," *Computational Mechanics*, Vol. 22, No. 2, pp. 117-127.

Atluri, S. N., and Zhu, T., 2000, "The Meshless Local Petrov-Galerkin (MLPG) Approach for Solving Problems in Elasto-Statics," *Computational Mechanics*, Vol. 25, Nos. 2-3, pp. 169-179.

Batra, R. C., and Ching, H. K., 2002, "Analysis of Elastodynamic Deformations Near a Crack-Notch Tip by the Meshless Local Petrov-Galerkin (MLPG) Method," *Computer Modeling in Engineering and Sciences*, Vol. 3, No. 6, pp. 717-730.

Belytschko, T., Krongauz, Y., Organ, D. J., Fleming, M., and Krysl, P., 1996, "Meshless Methods: An Overview and Recent Developments," *Computer Methods in Applied Mechanics and Engineering*, Vol. 139, pp. 3-47.

Belytschko, T., Liu, W. K., and Moran, B., 2000, *Nonlinear Finite Elements for Continua and Structures*, Wiley, Chichester, UK.

Belytschko, T., Lu, Y. Y., and Gu, L., 1994, "Element-Free Galerkin Methods," *International Journal for Numerical Methods in Engineering*, Vol. 37, pp. 229-256.

Chati, M. K., and Mukherjee, S., 2000, "The Boundary Node Method for Three-Dimensional Problems in Potential Theory," *International Journal for Numerical Methods in Engineering*, Vol. 47, No. 9, pp. 1523-1547.

Cheng, Z. Q., and Batra, R. C., 2000, "Deflection Relationships between the Homogeneous Kirchhoff Plate Theory and Different Functionally Graded Plate Theories," *Archive of Mechanics*, Vol. 52, No. 1, pp. 143-158.

Ching, H. K., and Batra, R. C., 2001, "Determination of Crack Tip Fields in Linear Elastostatics by the Meshless Local Petrov-Galerkin (MLPG) Method," *Computer Modeling in Engineering and Sciences*, Vol. 2, No. 2, pp. 273-289.

Delale, F., and Erdogan, F., 1983, "The Crack Problem for Nonhomogeneous Plane," *ASME Journal of Applied Mechanics*, Vol. 50, pp. 609-614.

Duarte, C. A., and Oden, J. T., 1996, "H-*p* Clouds – an *hp* Meshless Method," *Numerical Methods for Partial Differential Equations*, Vol. 12, No. 6, pp. 673-705.

Gu, Y. T., and Liu, G. R., 2001a, "A Meshless Local Petrov-Galerkin (MLPG) Method for Free and Forced Vibration Analyses for Solids," *Computational Mechanics*, Vol. 27, No. 3, pp. 188-198.

Gu, Y. T., and Liu, G. R., 2001b, "A Meshless Local Petrov-Galerkin (MLPG) Formulation for Static and Free Vibration Analysis of Thin Plates,"

Computer Modeling in Engineering and Sciences, Vol. 2, No. 4, pp. 463-476.

Hashin, Z., and Shtrikman, S., 1963, " A Variational Approach to the Theory of Elastic Behavior of Multiphase Materials," *Journal of the Mechanics and Physics of Solids*, Vol. 11, No. 2, pp127-140.

Hill, R., 1965, "A Self-Consistent Mechanics of Composite Materials," *Journal of the Mechanics and Physics of Solids*, Vol. 13, No. 2, pp. 213-222.

Jin, Z. H., and Batra, R. C., 1996, "Stress Intensity Relaxation at the Tip of an Edge Crack in a Functionally Graded Material Subjected to a Thermal Shock," *Journal of Thermal Stresses*, Vol. 19, pp. 317-339.

Jin, Z. H., and Noda, N., 1994, "Transient Thermal Stress Intensity Factors for a Crack in a Semi-Infinite Plane of a Functionally Gradient Material, " *International Journal of Solids and Structures*, Vol. 31, pp. 203-218.

Lancaster, P., and Salkauskas, K., 1981, "Surfaces Generated by Moving Least Squares Methods," *Mathematics of Computation*, Vol. 37, No. 155, pp. 141-158.

Lin, H., and Atluri, S. N., 2000, "Meshless Local Petrov-Galerkin (MLPG) Method for Convection-Diffusion Problems," *Computer Modeling in Engineering and Sciences*, Vol. 1, No. 2, pp. 45-60.

Liu, G. R., and Gu, Y. T., 2000, "Meshless Local Petrov-Galerkin (MLPG) Method in Combination with Finite Element and Boundary Element Approaches," *Computational Mechanics*, Vol. 26, No. 6, pp. 536-546.

Liu, G. R., and Gu, Y. T., 2001, "A Local Radial Point Interpolation Method (LR-PIM) for Free Vibration Analyses of 2-D Solids," *Journal of Sound and Vibration*, Vol. 246, No. 1, pp. 29-46.

Liu, W. K., Jun, S., and Zhang, Y. F., 1995, "Reproducing Kernel Particle Methods," *International Journal for Numerical Methods in Engineering*, Vol. 20, pp. 1081-1106.

Long, S., and Atluri, S. N., 2002, "A Meshless Local Petrov-Galerkin Method for Solving the Bending Problem of a Thin Plate," *Computer Modeling in Engineering and Sciences*, Vol. 3, No. 1, pp. 53-64.

Melenk, J. M., and Babuska, I., 1996, "The Partition of Unity Finite Element Method: Basic Theory and Applications," *Computer Methods in Applied Mechanics and Engineering*, Vol. 139, pp. 289-314.

Miyamoto, Y., Kaysser, W. A., Rabin, B. H., Kawasaki, A., and Ford, R. G., 1999, *Functionally Graded Materials: Design, Processing*, and Applications, Kluwer, MA, USA.

Mori, T., and Tanaka, K., 1973, "Average Stress in Matrix and Average Elastic Energy of Materials with Misfitting Inclusions," *Acta Metallurgic*a, Vol. 21, pp. 571-574.

Nayroles, B., Touzot, G., and Villon, P., 1992, "Generalizing the Finite Element Method: Diffuse Approximation and Diffuse Elements," *Computational Mechanics*, Vol. 10, pp. 307-318.

Newmark, N. M., 1959, "A Method of Computation for Structural Dynamics," *Journal of Engineering Mechanics Division*, ASCE, Vol. 85, No. EM3, pp. 67-94.

Noda, N., and Jin, Z. H., 1993, "Thermal Stress Intensity Factors for a Crack in a Strip of a Functionally Gradient Material," *International Journal of Solids and Structures*, Vol. 30, No. 8, pp. 1039-1056.

Qian, L. F., Batra, R. C., and Chen, L. M., 2003a, "Elastostatic Deformations of a Thick Plate by Using a Higher-Order Shear and Normal Deformable Plate Theory and Two Meshless Local Petrov-Galerkin (MLPG) Methods," *Computer Modeling in Engineering and Sciences*, Vol. 4, No. 1, pp. 161-175.

Qian, L. F., Batra, R. C., and Chen, L. M., 2003b, "Free and Forced Vibrations of Thick Rectangular Plates by Using Higher-Order Shear and Normal Deformable Plate Theory and Meshless Local Petrov-Galerkin (MLPG) Method," *Computer Modeling in Engineering and Sciences*, Vol. 4, No. 5, pp. 519-534.

Reddy, J. N., 2000, "Analysis of Functionally Graded Plates," *International Journal for Numerical Methods in Engineering*, Vol. 47, Nos. 1-3, pp. 663-684.

Sankar, B. V., 2001, "An Elasticity Solution for Functionally Graded Beams," *Composites Science and Technology*, Vol. 61, No. 5, pp. 689-696.

Suresh S., and Mortensen, A., 1998, *Fundamentals of Functionally Graded Materials*, IOM Communications, London, UK.

Tarn, J. Q., 2001, "Exact Solutions for Functionally Graded Anisotropic Cylinders Subjected to Thermal and Mechanical Loads," *International Journal of Solids and Structures*, Vol. 38, Nos. 46-47, pp. 8189-8206.

Vel, S. S., and Batra, R. C., 2002, "Exact Solution for Thermoelastic Deformations of Functionally Graded Thick Rectangular Plates," *AIAA Journal*, Vol. 40, No. 7, pp. 1421-1433.

Wakashima, K., and Tsukamoto, H., 1991, "Mean-Field Micromechanics Model and its Application to the Analysis of Thermomechanical Behaviour of Composite Materials," *Materials Science and Engineering A*, Vol. 146, Nos. 1-2, pp. 291-316.

Warlock, A., Ching, H. K., Kapila, A. K., and Batra, R. C., 2002, "Plane Strain Deformations of an Elastic Material Compressed in a Rough Rectangular Cavity," *International Journal of Engineering Science*, Vol. 40, No. 9, pp. 991-1010.

Manuscript Received: Aug. 18, 2003
Revision Received: Dec. 20, 2003
and Accepted: Jan. 15, 2004